The formation and characterization of three-dimensional gold nanocrystal superlattices

Michael G. Constantinides[I], Heinrich M. Jaeger[I], Xuefa Li[II], Jin Wang[II] and Xiao-Min Lin[*, III]

[I] The James Franck Institute, University of Chicago, 929 E 57th Street, Chicago, IL 60637, USA
[II] Advanced Photon Source, Argonne National Laboratory, 9700 South Cass Avenue, Argonne, IL 60439, USA
[III] Center for Nanoscale Materials, Argonne National Laboratory, 9700 South Cass Avenue, Argonne, IL 60439, USA

Received March 7, 2007; accepted September 25, 2007

Nanocrystals / Nanoparticles / Self-assembly / GISAXS / Supercrystals / Superlattices

Abstract. Highly-ordered, three-dimensional superlattices were self-assembled from dodecanethiol-ligated gold nanocrystals using a simple drop-drying technique. The superlattices had the shape of truncated pyramids (frustums) and reached lateral dimensions of several micrometers. The formation and thermal stability were studied by grazing-incidence small-angle X-ray scattering. We found that the superlattice frustums adopt an *hcp* packing structure. When annealed above 50 °C in vacuum, the lattices started to disorder and the average lattice spacing was observed to decrease. This could be associated with the onset of a ligand melting transition as well as the continuous desorption of ligands in vacuum.

1. Introduction

Developments in colloidal chemistry during the past decade have yielded many different types of nanocrystals with well controlled size, shape and monodispersity. These nanocrystals can be used as building blocks to create novel macroscopic crystalline materials, ie. superlattices, through self-assembly [1, 2]. An intriguing aspect of these new materials is that the properties of superlattices can potentially be tuned not only by the properties of the individual nanocrystal building blocks, but also by the coupling between them. Nanocrystal superlattices with well-controlled structure therefore could offer unique opportunities to study many interesting phenomena, such as the metal-insulator transition [1], resonant energy transfer [3] and plasmon propagation [4].

The most straightforward way to self-assemble nanocrystal superlattices is through evaporation of colloidal droplets. This approach has been applied to a variety of different materials, such as Au [5], CdSe [6], Ag [7], Fe_3O_4 [8, 9], and has also been extended to form more complex superlattices composed of several different inorganic building blocks [10, 11]. However, the size of superlattices produced by drop-casting and the degree of structural order reported in the literature vary significantly. This is largely due to the multitude of complex, non-equilibrium phenomena associated with the evaporation process. Dodecanethiol-ligated gold nanocrystal colloids offer a model system to understand the intrinsic mechanisms driving drying-mediated self-assembly. Highly monodispersed Au nanocrystals can be readily synthesized through a digestive ripening protocol [12] or using a size selective precipitation process [13]. These particles are stable in air and can be processed by repeated precipitations and solvent washes without degrading the sample.

We have shown previously that, using these nanocrystals, highly ordered two-dimensional (2D) nanocrystal monolayers and bilayers can be formed [14]. Recent *in situ* small angle X-ray scattering experiments [15] and optical microscopy studies [16] revealed that the formation of 2D superlattice structures occurs during the early stage of drying at the liquid-air interface of the evaporating droplet. This early stage corresponds to rapid evaporation and far-from-equilibrium conditions. In this paper, we investigate the opposite limit of very slow evaporation. We show that, with high concentration of nanocrystals, slow evaporation condition leads to the formation of three dimensional (3D) superlattices that reach lateral extents of several microns and heights of hundreds of particle diameters. We investigate their structure and thermal stability upon heating the sample to 200 °C.

2. Formation of 3D nanocrystal superlattices

In earlier work, we found that the formation of highly ordered 2D structures during drop-casting is kinetically driven because of the relatively slow diffusion of nanoparticles compared to the fast moving liquid-air interface during to solvent evaporation [16]. Thus, the majority of nanocrystals become trapped at the 2D liquid-air interface before a significant number of 3D nucleation sites had a chance to form inside the colloidal drop. However, if the evaporation rate is decreased significantly, 2D crystallization at the liquid-air interface will be suppressed because the the diffusion of nanocrystals away from the interface

* Correspondence author (e-mail: xmlin@anl.gov)

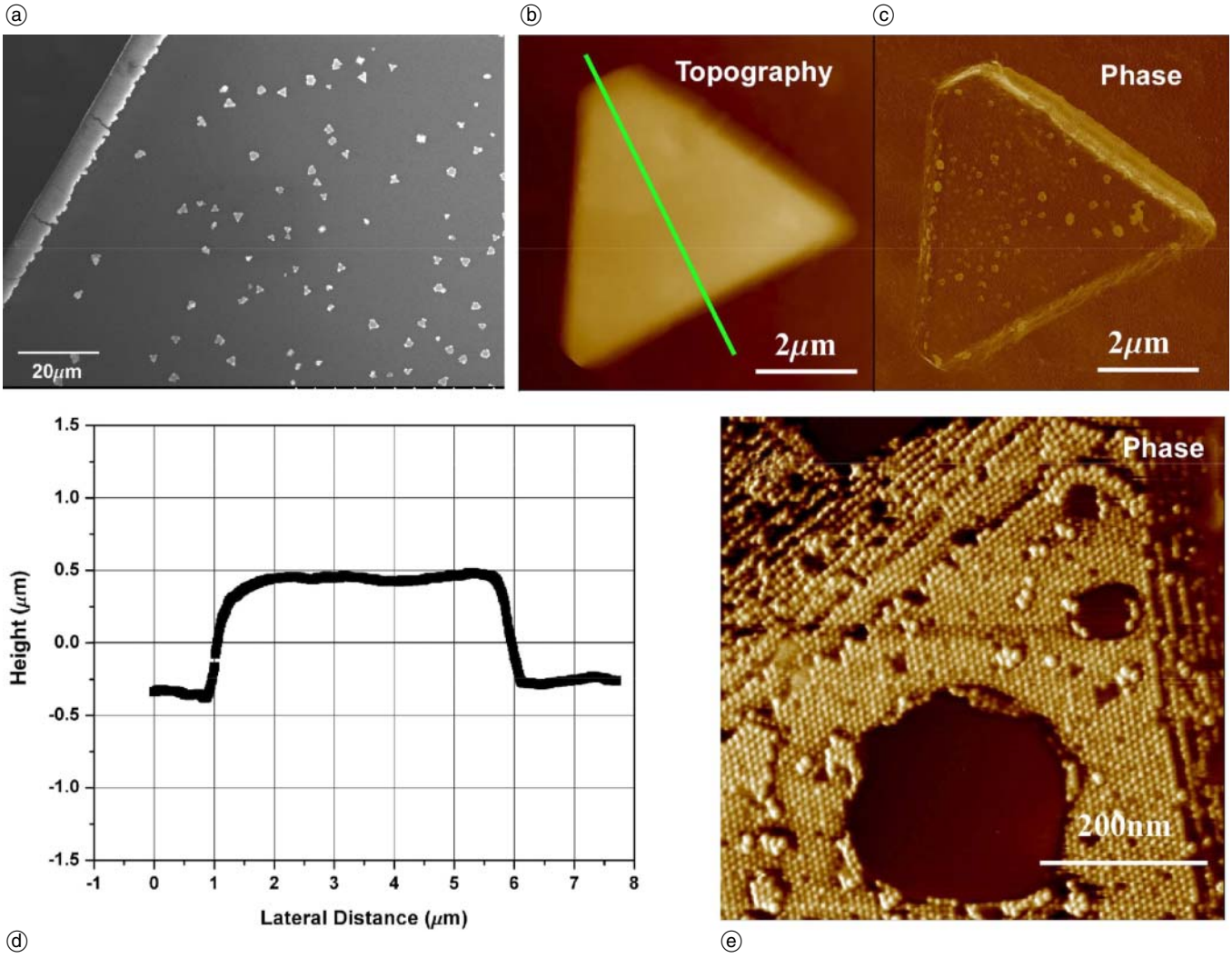

Fig. 1. (**a**) SEM image of 3D frustrum-shaped gold nanocrystal superlattices formed on a SiN substrate. (**b–c**) Low resolution AFM topography and phase image of a single superlattice (**d**) Cross-section height profile along the line shown in panel *b*. (**e**) High resolution AFM phase image of a single superlattice showing a terrace-like surface structure.

becomes important. Thus, the density of nanocrystals inside the droplet will grow until it exceeds the critical concentration for the nucleation of 3D superlattices. Based on this approach, we have developed a method for inducing the self-assembly of highly-ordered 3D superlattices directly on solid substrates.

We used monodispersed dodecanethiol-ligated gold nanocrystals with an average diameter of 6 nm, synthesized through a digestive ripening procedure developed earlier [12]. The particles were dissolved in toluene, and the concentration was adjusted to approximately 10^{13} mL^{-1}. To insure that the coverage of the ligand shell surrounding the particles was complete, and therefore the interparticle spacing well-defined, excess dodecanethiol was added to the suspension at a volume concentration of 0.1%. The suspension was allowed to sit undisturbed for 72 hours before the experiments. As verified by dynamic light scattering (DLS), this led to the formation of small (∼100 nm diameter) superlattice seeds. 10 μl of colloidal suspension was deposited onto a rectangular silicon nitride substrate (3×4 mm^2), and allowed to dry very slowly in a saturated toluene vapor environment (evaporation rate < 0.22 mg/min).

Figure 1a shows a scanning electron microscope (SEM) image of the sample surface after the colloidal suspension had dried completely. Besides the multilayer structures at the edge of the substrate, a large number of self-assembled structures with well-defined edges and often triangular shapes are apparent. Closer inspection, using tapping mode atomic force microscopy (AFM), reveals highly-ordered superlattices with mesa-like tops and terraced sides similar to truncated pyramids (frustums). Typical lateral dimensions of these structures are 5–6 micrometers (Figs. 1b–c). The average height of the frustums is ∼1 μm (Fig. 1d), which is typically smaller than their lateral dimension. Figure 1e gives a detailed view of a corner of one of these frustums, showing the nearly perfect stacking and registry of the particle layers in the [111] direction. The three dark circular areas are unevaporated excess dodecanethiol droplets. Figure 1e is a AFM phase image in which darker color does not correspond to lower-lying topographic features; the AFM height image, taken simultaneously with the phase image, shows that the dodecanethiol droplet indeed bulges out above the superlattice top surface. There are also occasional frustums containing a few individual superlattice crystals fused together.

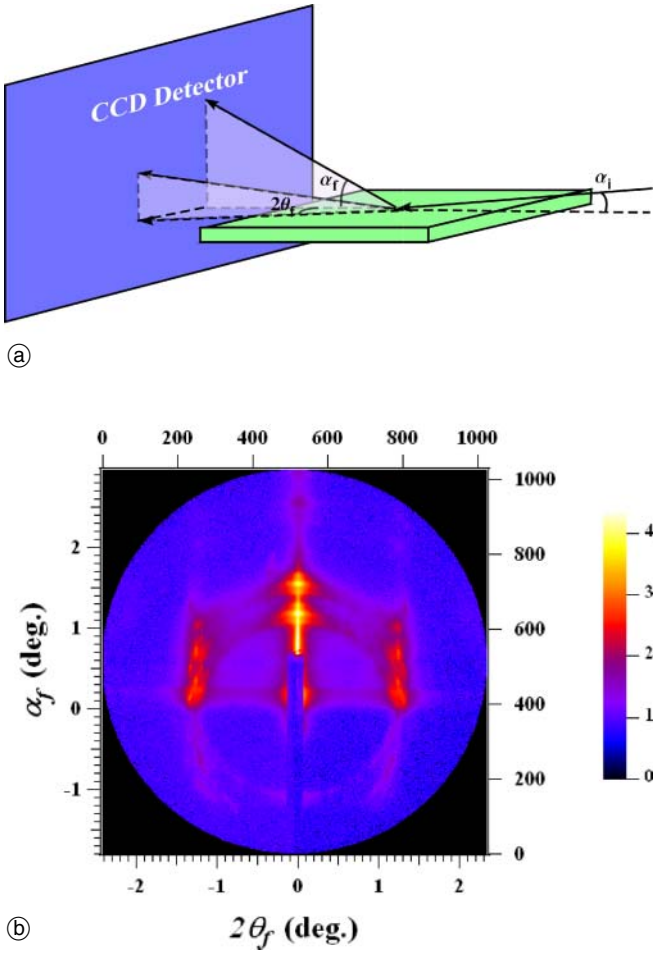

Fig. 2. (**a**) Schematic diagram of GISAXS setup. (**b**) GISAXS scattering pattern of 3D frustum-shaped superlattices at room temperature with incident angle $\alpha_i = 0.2^\circ$.

3. Superlattice structure and thermal stability

Since the coverage of the substrate with superlattices was sparse, we used grazing-incidence small-angle X-ray scattering (GISAXS) to characterize the superlattice structure. The grazing-incidence geometry expands the X-ray beam's footprint on the substrate, allowing for a larger surface area to be sampled. The GISAXS experiments were conducted at the 8-ID beamline of the Advanced Photon Source (APS). The incident synchrotron X-ray beam was energy-filtered to 7.45 keV by a double-crystal monochromator while two sets of horizontal (H) and vertical (V) slits were used to define the beam size to 0.2 (H) $\times$0.05 (V) mm^2. The samples was placed on a holder in a vacuum chamber, which was subsequently pumped down to 10^{-6} torr. After aligning the sample parallel to the X-ray beam, the incidence angle (α_i) was changed slightly by rotating the sample stage. Figure 2 shows the schematic diagram of the setup as well as the scattering pattern on the CCD detector at an incident angle $\alpha_i = 0.2^\circ$. Two concentric circular scattering patterns can be seen, which correspond to the diffraction from the superlattice by both the direct incident beam and the reflected beam from the substrate. The strong diffraction in the specular direction is due to the stacking of mutilayers of nanocrystals perpendicular to the substrate, whereas the scattering in the lateral direction mostly contains information regarding the in-plane ordering. Because the separation between the two sets of diffraction patterns in the lateral direction is small, it is more convenient to analyze the diffraction pattern in the specular direction. Figure 3 shows the intensity profile in the specular direction for various incident angles $\alpha_i = 0.1^\circ - 0.3^\circ$, plotted in terms of scattering wavevector q_α. The q_α value is only meaningful for the incident beam because the $q_\alpha = 0$ point is where the incident wavevector intercept the the detector plane. The set of diffraction

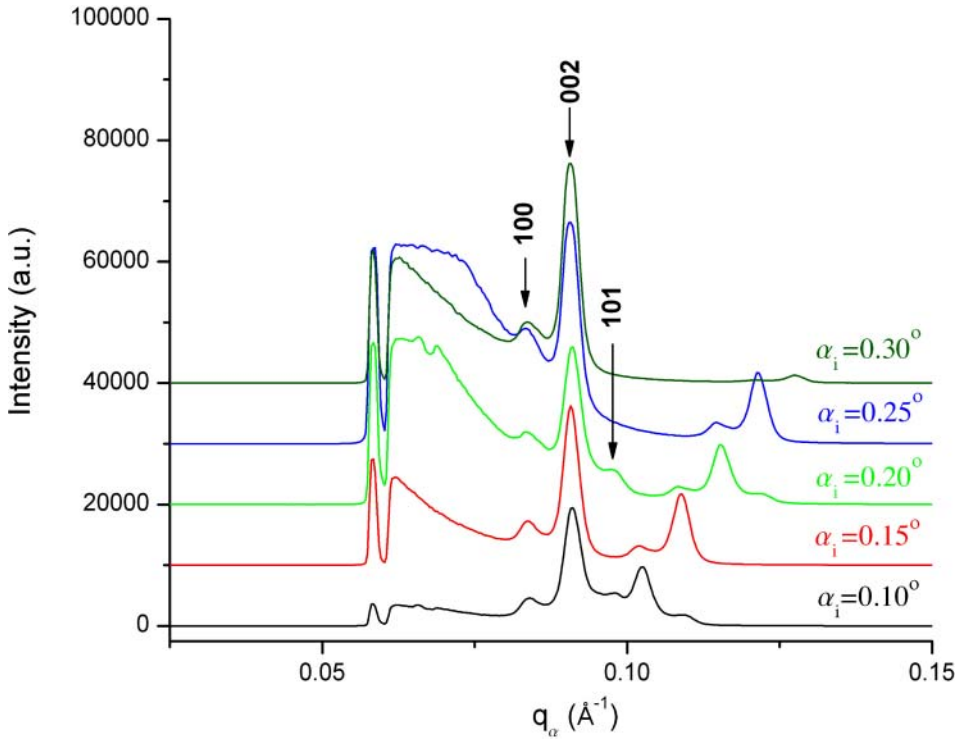

Fig. 3. The intensity profile of scattering pattern in specular direction ($2\theta_f = 0$) with different incident angles (α_i). The sample was kept at room temperature.

peaks that correspond to the reflected beam changes with the incident angle. At certain incident angles $\alpha_i = 0.1°$, 0.2°, three peaks are visible. This allows us to conclude that the supercrystal structure is hexagonal-close-packed (*hcp*) with unit cell parameter $a = 84.6$ Å, $c = 135.1$ Å. The ratio $c/a = 1.60$ is slightly smaller than the theoretical value for hard spheres (1.63). The peak corresponding to {101} reflection is weak, and disappears or reappears as we move the sample laterally with respect to the X-ray beam, indicating the degree of ordering varies slightly from one superlattice to another.

Monodisperse hard spheres can form both face-centered cubic (*fcc*) and *hcp* lattices with the identical packing density (0.74) as a result of entropic effects [17]. The free energy for both structures is nearly identical [18]. Ligated colloidal nanocrystals, on other hand, only approximately behave like hard spheres, and the repulsive interactions between shells of ligand molecules belonging to neighboring particles depend on both the ligand length and the packing density [19]. In these systems, both face-centered cubic and hexagonal structures have been observed, as have lower symmetry structures, although less frequently [6, 7, 19, 20, 21]. Whetten *et al.* have parameterized the accompanying structural transitions by introducing a characteristic ratio $\chi = \frac{2L}{D}$, where L is the extended ligand chain length and D is the particle core diameter [26]. As the value of χ increases, the most stable structures evolve in the sequence from *hcp* to *fcc* to body-centered cubic/tetragonal (*bcc*/*bct*). The *fcc* to *bcc*/*bct* transition was well characterized using different size gold clusters coated with C_6 thiol. However, the transition from *hcp* to *fcc* is more ambiguous. Experimental results from several groups showed that for colloids with similar sizes, composition and ligand coating, *fcc* and *hcp* can both be observed, sometimes even in the same sample [6, 7, 20, 21]. For the gold nanocrystals used in our experiments ($D = 6$ nm, $L \sim 1.5$ nm), $\chi = 0.59$, which would place the superlattices in the *fcc*/*hcp* region. The GISAXS data in Fig. 3 shows that the superlattices made from these nanocrystals have *hcp* structure.

Our AFM studies have shown the 3D superlattices contain terrace-like sides, with essentially flat tops. Furthermore, we found that the tops for different crystals are nearly at the same height, suggesting an assembly mechanism that occurs during the late stages of drying where the particle concentration is high and the liquid level is close to the substrate. Under these conditions, superlattice seedlings have settled on the substrate and their vertical growth is limited by the height of the liquid level. As drying proceeds, the level drops and further aggregation of material can only occur along the sides of the frustums, giving rise to the terracing and simultaneously guaranteeing registry. The triangular shape of the 3D superlattice is also reminiscent of the triangular shaped atomic crystals formed by several metals, such as Au, Ag and Pb [22–24]. However, instead of having atoms as the basic building blocks, the superlattices are made of nanoparticles, which are an order of magnitude larger in size. For atomic crystals with *fcc* and *hcp* stacking, twinning plane defects are energetically quite favorable to be incorporated in the early nuclei when the growth is along ⟨111⟩ directions. These defects subsequently direct the growth of crystals into anisotropic shape because of the reentrant grooves formed by the twinning planes are highly favorable sites for further attachment of new atoms [23, 25]. In a similar mechanism, twinning planes in 3D superlattices could also induce anisotropic growth that leads to the formation of triangular shaped structure.

An important aspect related to the application of nanocrystal superlattices is their thermal stability. The *in situ* GISAXS measurements allowed us to monitor structural changes while annealing the sample to different temperatures up to 200 °C. Figure 4 shows the change of {002}

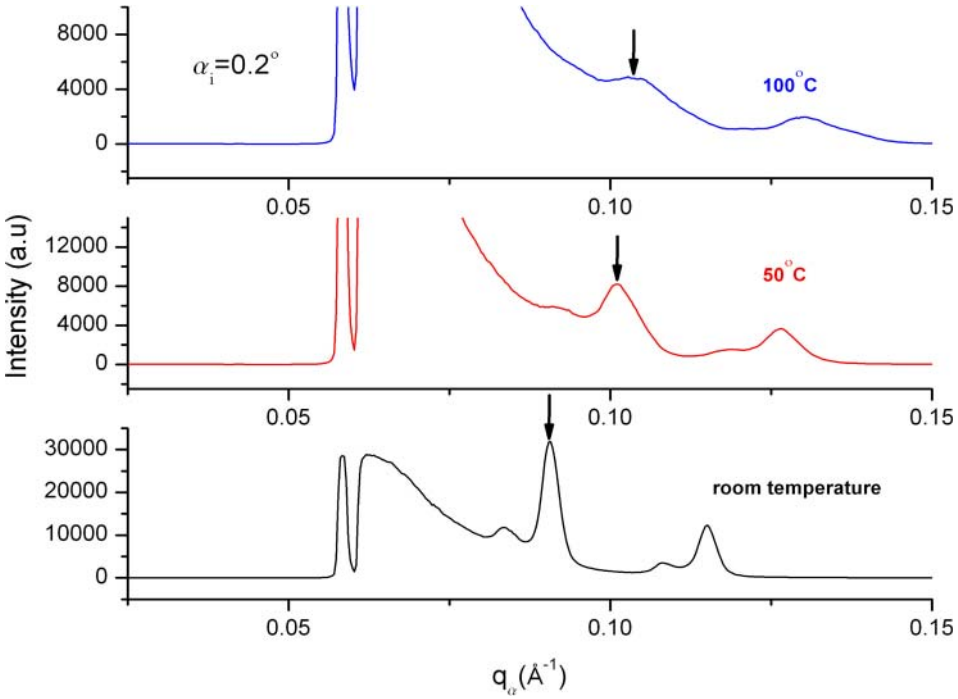

Fig. 4. The change of scattering pattern in specular direction ($2\theta_f = 0$) when the sample is heated at three different temperatures (incident angle $\alpha_i = 0.2°$).

reflections at three different temperatures. We found that, with sample in vacuum, even at 50 °C, there is a significant decrease of the intensity and a broadening of the {002} peak. The peak position also shifts to a larger q value. This indicates that the average lattice spacing decreases dramatically (11% change), accompanied by an increase of lattice disorder. Upon cooling the sample from 200 °C back to room temperature, the diffraction patterned did not recover its original form, which indicates irreversible structural changes to the superlattices.

We speculate that the structural changes around 50 °C could be associated with the melting of alkanethiol molecules at the nanocrystal surface. Based on molecular dynamics simulations, Luedtke and Landman proposed that the thiol molecules between neighboring nanocrystals inside a superlattice form bundles at low temperatures [27]. At higher temperatures, they predict a first-order melting transition of thiol molecules occurs through intramolecular conformation changes. For the small thiolated gold clusters $(Au_{140}(C_{12}H_{25}S)_{62})$ used in their simulation, the melting transition was predicted to be ~ -10 °C. Experiments by Fenter *et al.* on extended 2D gold surface, on the other hand, showed that the melting transition for dodecanethiol molecules occurs near 50 °C [28]. Because of the large particle size used in our experiments (6 nm), the thiol molecules could behave closer to the situation on the extended metal surface. Furthermore, the excess molecules that are not bound to nanoparticle surface are more easily removed by vacuum at elevated temperatures. At temperature higher than ∼120 °C, even ligand molecules that are directly bound to gold surfaces begin to desorb [29, 30]. All these effects could cause disorder in the superlattices, which leads to sintering of particles and irreversible structural disorder in the superlattice. This explains the observed continuous broadening of the {002} peak when the sample temperatures is raised above 50 °C. In the meantime, the average lattice spacing decreases, which is caused by the reduced range of steric repulsive interaction during the ligand melting and desorption.

We also note that the experiments presented above were performed under vacuum during which the ligand molecules were being actively pumped off. Under ambient conditions, the order-disorder transition temperature could be much higher. This is in accord with preliminary X-ray results we obtained by comparing the thermal stability of 2D superlattices both in air and in vacuum [31]. This is also consistent with the recent observations on freely-suspended monolayer superlattices in air, which are found to be stable even up to 140 °C [32].

4. Conclusion

Because the lattice spacings in nanocrystal superlattices are on the order of a few nanometers, GISAXS has proven to be an effective technique to study the formation and thermal stability of these systems. The structural transformation of superlattices was shown to be in line with the melting and desorption of ligands at high temperature, which eventually leads to local sintering of nanocrystals. However, the thermal stability of superlattices could also depend on the particle size and surface ligand length. Thus, a more systematic study of the dependence on these parameters would help to control the structure and thermal stability of 3D superlattices. This work (including the use of the APS) was supported by DOE, BES-Materials Sciences, under Contract DE-AC02-06CH11357, by the University of Chicago – Argonne National Laboratory Consortium for Nanoscience Research (CNR), and by the MRSEC program of the NSF under DMR-0213745. M. Constantinides acknowledges support from the MRSEC REU program. We also thank Dr. Qiti Guo and the Argonne Electron Microscopy Center for experimental assistance.

References

[1] Collier, C. P.; Vossmeyer, T.; Heath, J. R.: Nanocrystal superlattices. Annu. Rev. Phys. Chem. **349** (1998) 71.
[2] Weller, H.: Self-Organized superlattices of nanoparticles. Angew. Chem. Int. Ed. Engl. **35** (1996) 1079.
[3] Murray, C. B.; Kagan, C. R.; Bawendi, M. G.: Synthesis and characterization of monodisperse nanocrystals and close-packed nanocrystal assemblies. Annu. Rev. Mater. Sci. **30** (2000) 545.
[4] Maier, S. A.; Brongersma, M. L.; Kik, P. G.; Atwater, H. A.: Observation of near-field coupling in metal nanoparticle chains using far-field polarization spectroscopy. Physical Review B**65** (2002) 193408.
[5] Kiely, C. J.; Fink, J.; Brust, M.; Bethell, D.; Schiffrin, D. J.: Spontaneous ordering of bimodal ensembles of nanoscopic gold clusters. Nature **396** (1998) 444.
[6] Talapin, D. V.; Shevchenko, E. V.; Gaponik, N.; Radtchenko, I. L.; Kornowski, A.; Haase, M.; Rogach, A. L.; Weller, H.: Reply: self-assembly of monodisperse nanocrystals into faceted crystal superlattices. Adv. Mater. **17** (2005) 1325.
[7] Harfenist, S. A.; Wang, Z. L.; Whetten, R. L.; Vezmar, I.; Alvarez, M. M.: Three-dimensional hexagonal close-packed superlattice of passivated Ag nanocrystals. Adv. Mater. **9** (1997) 817.
[8] Bentzon, M. D.; van Wonterghem, J.; Mørup, S.; Thölén, A.; Koch, C. J. W.: Ordered aggregates of ultrafine iron oxide particles: 'super crystals'. Philo. Mag. B**60** (1989) 169.
[9] Park, J.; An, K.; Hwang, Y.; Park, J.; Noh, H.; Kim, J.; Park, J.; Hwang, N.; Hyeon, T.: Ultra-largescale syntheses of monodisperse nanocrystals. Nature Mater. **3** (2004) 891.
[10] Kalsin, A.-M.; Fialkowski, M.; Paszewski, M.; Smoukov, S. K.; Bishop, K. J.; Grzybowski, B. A.: Electrostatic self-assembly of binary nanoparticle crystals with a diamond-like lattice. Science **312** (2006) 420.
[11] Urban, J. J.; Talapin, D. V.; Shevchenko, E. V.; Kagan, C. R.; Murray, C. B.: Synergism in binary nanocrystal superlattices leads to enhanced *p*-type conductivity in self-assembled PbTe/Ag_2Te thin films. Nature Mater. **6** (2007) 115.
[12] Lin, X. M.; Sorensen, C. M.; Klabunde, K. J.: Digestive ripening, nanophase segregation and superlattice formation in gold nanocrystal colloids. J. Nanoparticle Res. **2** (2000) 157.
[13] Brust, M.; Walker, M.; Bethell, D.; Schiffrin, D. J.; Whyman, R.: Synthesis of thiol-derivatised gold nanoparticles in a two-phase liquid-liquid system. J. Chem. Soc., Chem. Commun. (1994) 801.
[14] Lin, X. M.; Jaeger, H. M.; Sorensen, C. M.; Klabunde, K. J.: Formation of long-range-ordered nanocrystal superlattices on silicon nitride substrates. J. Phys. Chem. B**105** (2001) 3353.
[15] Narayanan, S.; Wang, J.; Lin, X. M.: Dynamical self-assembly of nanocrystal superlattices during colloidal droplet evaporation by *in situ* small angle X-ray scattering. Phys. Rev. Lett. **93** (2004) 135503.
[16] Bigioni, T. P.; Lin, X. M.; Nguyen, T. T.; Corwin, E. I.; Witten, T. A.; Jaeger, H. M.: Kinetically driven self assembly of highly ordered nanoparticle monolayers. Nature Materials **5** (2006) 265.
[17] Woodcock, L. V.: Entropy difference between the face-centred cubic and hexagonal close-packed crystal structures. Nature **385** (1997) 141.
[18] Adler, B. J.; Carter, B. P.; Young, D. A: Crystal transformation for hard spheres. Phys. Rev. **183** (1969) 831.

[19] Korgel, B. A.; Fullam, S.; Connolly, S.; Fitzmaurice, D.: Assembly and self-organization of silver nanocrystal superlattices: Ordered "Soft Spheres". J. Phys. Chem. B**102** (1998) 8379.
[20] Stoeva, S. I.; Prasad, B. L. V.; Uma, S.; Stoimenov, P. K.; Zaikovski, V.; Sorensen, C. M.; Klabunde, K. J.: Face-centered cubic and hexagonal closed-packed nanocrystal superlattices of gold nanoparticles prepared by different methods. J. Phys. Chem. B**107** (2003) 7441.
[21] Harfenist, S. A.; Wang, Z. L.; Alvarez, M. M.; Vezmar, I.; Whetten, R. L.: Highly oriented molecular Ag nanocrystal arrays. J. Phys. Chem. **100** (1996) 13904.
[22] Jin, R.; Cao, Y.; Mirkin, C. A.; Kelly, K. L.; Schatz, G. C.; Zhen, J. G.: Photoinduced conversion of silver nanospheres to nanoprisms. Science **294** (2001) 1901.
[23] Kirkland, A. I.; Jefferson, D. A.; Diff, D. G.; Edwards, P. P.; Gameson, I.; Johnson, B. F. G.; Smith, D.: Structural studies of trigonal lamellar particles of gold and silver. J. Proc. R. Soc. London, Ser. A**440** (1993) 589.
[24] Lin, X. M.; Claus, H.; Welp, U.; Beloborodov, I. S.; Kwok, W.-K.; Crabtree, G. W.; Jaeger, H. M.: Growth and properties of superconducting anisotropic lead nanoprisms. J. Phys. Chem. C. **111** (2007) 3548.
[25] Lofton, C.; Sigmund W.: Mechanisms controlling crystal habits of gold and silver colloids. Adv. Func. Mater. **15** (2005) 1197.
[26] Whetten, R. L.; Shafigullin, M. N.; Khoury, J. T.; Schaaff, T. G.; Vezmar, I.; Alvarez, M. M.; Wilkinson, A.: Crystal structures of molecular gold nanocyrstal arrays. Acc. Chem. Res. **32** (1999) 397.
[27] Luedtke, W. D; Landman, U.: Structure, dynamics, and thermodynamics of passivated gold nanocrystallites and their assemblies. J. Phys. Chem. **100** (1996) 13323.
[28] Fenter, P.; Eisenberger, P.; Liang, K. S.: Chainlength dependence of the structures and phases of $CH_3(CH_2)_{n-1}SH$ self-assembled on Au(111). Phys. Rev. Lett. **70** (1993) 2447.
[29] Kondoh, H.; Lodama, C.; Sumida, H.; Nozoye, H.: Molecular processes of adsorption and desorption of alkanethiol monolayers on Au(111). J. Chem. Phys. **111** (1999) 1175.
[30] Delamarche, E.; Michel, B.; Kang, H.; Gerber, Ch.: Thermal stability of self-assembled monolayers. Langmuir **10** (1994) 4103.
[31] To be published.
[32] Mueggenburg, K. E.; Lin, X. M.; Goldsmith, R. H.; Jaeger, H. M.: Elastic membranes of close-packed nanoparticle arrays. Nature Materials **6** (2007) 656.